Myocardial Infarction Area Quantification using High-Resolution SPECT Images in Rats

Luciano Fonseca Lemos de Oliveira[1], Jorge Mejia[2], Eduardo Elias Vieira de Carvalho[1], Renata Maria Lataro[1], Sarita Nasbine Frassetto[1], Rubens Fazan Jr.[3], Hélio Cesar Salgado[3], Orfa Yineth Galvis-Alonso[2], Marcus Vinícius Simões[1]

Divisão de Cardiologia, Departamento de Clínica Médica, Faculdade de Medicina de Ribeirão Preto, Universidade de São Paulo[1], Ribeirão Preto, SP; Faculdade de Medicina de São José do Rio Preto[2], São José do Rio Preto, SP; Departamento de Fisiologia, Faculdade de Medicina de Ribeirão Preto, Universidade de São Paulo[3], Ribeirão Preto, SP – Brazil

Abstract

Background: Imaging techniques enable in vivo sequential assessment of the morphology and function of animal organs in experimental models. We developed a device for high-resolution single photon emission computed tomography (SPECT) imaging to upgrade a clinical gamma-camera, based on pinhole collimator.

Objective: To determine the accuracy of this system for quantification of myocardial infarct area in rats.

Methods: Thirteen male Wistar rats (250 g) underwent experimental myocardial infarction by occlusion of the left coronary artery. After 4 weeks, SPECT images were acquired 1.5 hours after intravenous injection of 555 MBq of 99mTc-Sestamibi. The tomographic reconstruction was performed by using specially developed software based on the Maximum Likelihood algorithm. The analysis of the data included the correlation between the area of perfusion defects detected by scintigraphy and extent of myocardial fibrosis assessed by histology.

Results: The images showed a high target organ/background ratio with adequate visualization of the left ventricular walls and cavity. All animals presenting infarction areas were correctly identified by the perfusion images. There was no difference of the infarct area as measured by SPECT (21.1 ± 21.2%) and by histology (21.7 ± 22.0%; p=0.45). There was a strong correlation between individual values of the area of infarction measured by these two methods.

Conclusion: The developed system presented adequate spatial resolution and high accuracy for the detection and quantification of myocardial infarction areas, consisting in a low cost and versatile option for high-resolution SPECT imaging of small rodents. (Arq Bras Cardiol. 2013;101(1):59-67)

Keywords: Myocardial Infarction; Rats; Tomography, Emission-Computed;

Introduction

In the last decades, lab animals have become important tools in pre-clinical research[1]. In Cardiology, small animals have been successfully used for reproducing various cardiac disease models and their results have allowed the study of new drugs, as well as the study of cardiac disease physiopathological mechanisms[2-5].

On exploring of these animal models, although many experimental variables can be evaluated in vivo, in the majority of cases the animal must be sacrificed and the organ of interest excised and processed for obtaining results. This process eliminates the possibility of multiple evaluations along the time. On the other hand, the recent development of in vivo imaging techniques in small animals allowed the non-invasive sequential assessment of organ structure and function, saving time and animals and reducing cost.

The equipments in clinical use, based in ultrasond and magnetic resonance imaging, show sufficient sensivity and spatial resolution for imaging small animals organs, whose linear dimensions are, in average, 10 to 30 times smaller than that of human organs. However, conventional clinical SPECT (single-photon emission computed tomography) equipment allows spatial resolution of approximately 6 mm. This is not appropriate for imaging small animals' organs, for which the required spatial resolution is approximately 1 mm.

Our research group has recently described the implementation of a high-definition SPECT imaging system based on a pinhole collimator (with only one hole), a rotational support system for the small animal and appropriate software tools adapted to a gamma chamber for clinical use[6,7]. The objective of the present study was to validate this system for quantification in vivo of the myocardial fibrosis area in an experimental model of myocardial infarct in rats that uses as gold standard the in vitro histopathologic infarct measurement.

Mailing Address: Marcus Vinicius Simões •
Divisão de Cardiologia - Hospital das Clínicas da Faculdade de Medicina de Ribeirão Preto da Universidade de São Paulo
Av. Bandeirantes 3900 - Postal Code: 14048-900 - Ribeirão Preto - São Paulo
Email: msimoes@fmrp.usp.br
Manuscript received September 01, 2012; revised manuscript September 17, 2012 , accepted March 06, 2013.

DOI: 10.5935/abc.20130110

Methods

Construction and adaptation of the tomographic images acquisition system

A clinical gamma chamber (DST/Sopha Medical Vision, Twinsburg, Ohio, USA) was adapted by the construction of a shielding system that allowed the fixation of a 1.5 mm diameter simple orifice collimator, with a 150° total opening angle. This shielding system was pyramid-shaped and covered with a 6 mm lead mantle which was adequate for photons in the range of 150 keV. Additionally, a cylindrical support was developed for positioning the animal. This support is coupled to a motorized system, which allowed rotating the target to different angular positions, according to the number of projections to be registered throughout the 360° tomographic acquisition. Synchronized with the dynamic acquisition protocol of the gamma chamber, the projection sequence was registered and stored in DICOM format. The hardware set is illustrated on Figure 1.

Reconstruction software implementation

After acquiring the projections, the registered images were exported in DICOM format to a personal computer and were then processed for obtaining a tridimensional model for the radioactive drug distribution within the target [7]. In order to do this, we have developed an iterative image reconstruction software, based on the Maximum Likelihood algorithm[8]. The mathematical details of the iterative reconstruction calculations were published previously[7]. Even though the iterative reconstruction is slower than the filtered backprojection classic algorithm, it produces better quality images, in terms of the signal-noise rate and spatial resolution, and allows better modeling of the physical process involved in image acquisition[9,10]. The tool was implemented in C language, using a freeware Dev-V++ compiler (Bloodshed Software). The freeware Amide Medical Image Data Examiner[11] was used for the final visualization of the reconstructions.

Phantom Images

In order to verify the system's tomographic spatial resolution, hot bar phantom images were acquired. This phantom consists in four sets of cylindrical spaces with different diameters (1, 2, 3 and 4 mm), filled with sodium pertechnetate and separated by a distance equal to two times their diameter (Figure 2A). The same parameters employed for image acquisition of the experimental animals were used in the acquisition of the phantom images.

Experimental animals

After the approval of our institution's Ethical Committee in Animal Experimentation, the experiments were performed with 15 male Wistar rats weighing initially 250 g. The animals were provided by the central biotery of the same institution, kept in a climatized animal house, with free access to water and standard food, and submitted to a 12 hour light/shadow rhythm with controlled temperature. In all the procedures, maximum effort was done to avoid unnecessary suffering of the animals.

Experimental myocardial infarction induction

Experimental myocardial infarct was induced in 13 animals using the method described by Pfeffer et al[12], with slight modifications. Two animals were maintained as non-infarct controls. The surgical procedures were performed under anesthesia with ketamine (50 mg/kg IM, União Química Farmacêutica Nacional S/A, Embu-Guaçu, SP, Brasil) and xylazine (10 mg/kg IM, HertapeCalier Saúde Animal S/A, Juatuba, MG, Brasil) and orotracheal intubation for mechanical ventilation (Advanced Safety Ventilator, Harvard Apparatus, MA1 55-7059, Holliston, MA, USA). After that, the heart was exposed by an incision in the third left intercostal space and the anterior descendent branch of the left coronary artery was identified and ligated with a polyester thread (4-0, Ethicon, São José dos Campos, SP, Brasil). After that, the thorax was closed and the animals taken to our institution's Physiology Department Biotery for recovery.

Myocardial perfusion images acquisition

The animals were submitted to imaging 4 weeks after the experimental myocardial infarct induction. For the imaging protocol, the animals were anesthetized with a combination of ketamine and xylazine (50 e 5 mg/kg, respectively). A 555 MBq de 99mTc-Sestamibi activity was injected in the tail vein. Ninety minutes after the injections, the animals were anesthetized again with ketamine and xylazine (75 and 7.5 mg/kg, respectively) and positioned in the imaging system.

Thirty-six projections, equally spaced within 360°, were obtained in all imaging protocols. The projections were recorded in a 128 x128 matrix, each element with a 3.4 mm x 3.4 mm area. A 6.3X magnification factor was adopted for all experiments, corresponding to a lateral dimension of the volumetric picture element (or voxel) of 0.54 mm. The imaging time was 30 seconds for each projection, totaling approximately 21 minutes per animal.

No deaths were recorded in association to imaging within 4 weeks of the infarction.

Myocardial perfusion images processing and analysis

After reconstructing SPECT images with an iteractive reconstruction algorithm, the image was properly rotated and tomographic slices were selected from the short, long vertical and long horizontal axis. The images were normalized for the myocardial pixel with the maximum uptake value within the volume and submitted to visual analysis.

Four short axis tomographic slices from different levels within the left ventricular chamber were used for quantifying the perfusional defect in SPECT images: one apical slice, two medium-ventricular slices and one basal slice. Using ImageJ (a free image processing software), the intensity profile was determined at the left ventricle (LV) myocardial circumference. The areas with perfusion defects were identified by the presence of pixels with uptake values below 50% in comparison to the pixel showing the maximum caption accumulation in the myocardium. The total extension of the myocardial perfusion defect was expressed as a LV area percentage, and calculated by dividing the total pixel number with uptake < 50% (from the four slices) by the total pixel number of the LV circumferential profile in the four tomographic slices that were analyzed, multiplied by one hundred.

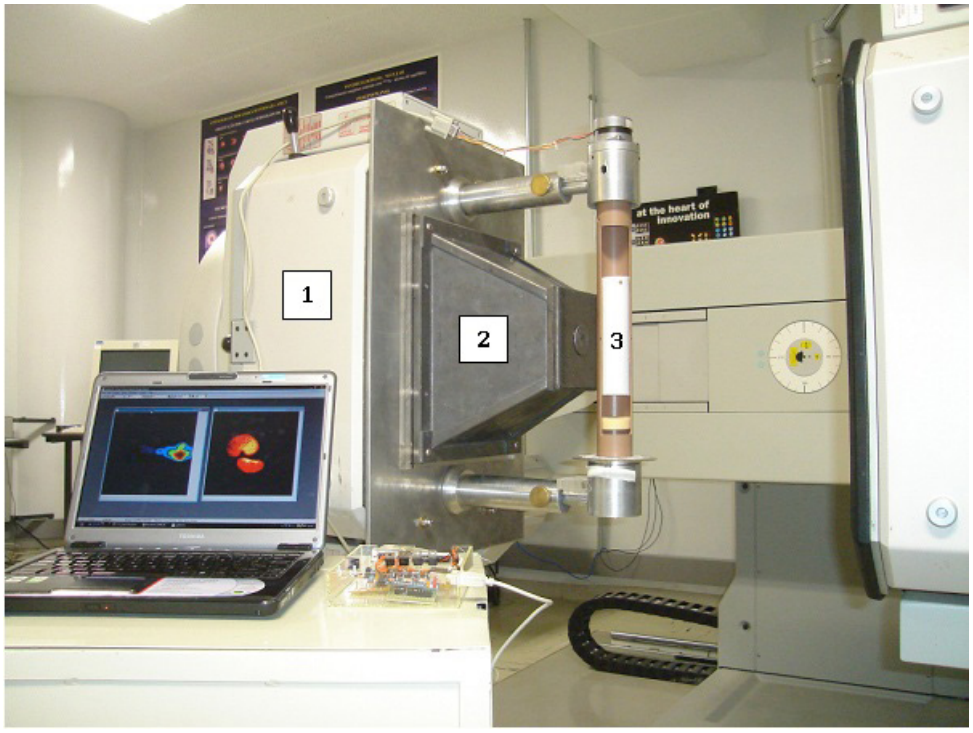

Figure 1 – *System positioned at one of the two heads of the Sopha/DST gamma-chamber. Coupled by an electromechanical mechanism, the system can be attached to different equipment. Besides, it allows imaging of mice to bigger rats, after simple system alterations. (1) Gamma-chamber detector. (2) Pyramid-shaped pinhole collimator support, (3) Rotational support for containing the small animal during imaging coupled to a step machine.*

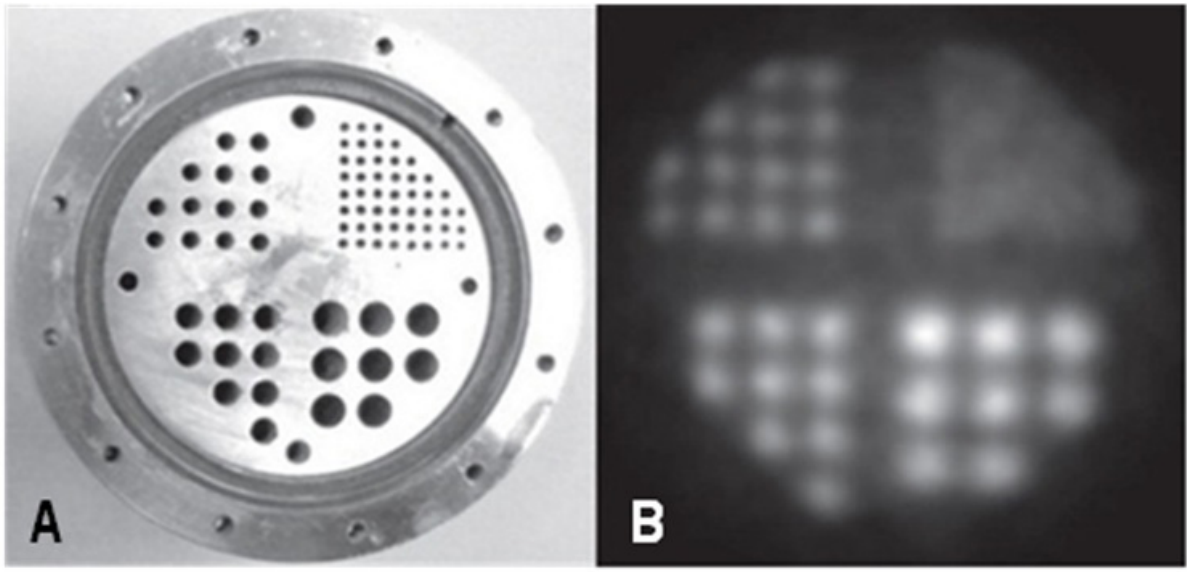

Figure 2 – *(A) The micro-Jaszczak phantom especially built and used in the study. Groups of cylindrical wells, with an internal diameter of 1-4 mm, can be seen. (B) Tomographic slice reconstructed perpendicularly to the phantom's long axis. The visual spatial resolution limit of the "hot bars" ranges from 1-2 mm.*

A single investigator, blind to the histologic analysis results, was responsible for the quantitative image processing.

Histology

For histopathologic analysis after euthanasia, the heart was rapidly excised and fixed in 10% formaldehyde for 24 hours, and, afterwards, transferred to 70% alcohol. The samples were progressively dehydrated and embedded in paraffin. Histologic slices were produced following the plane perpendicular to the heart's long axis, in order to reproduce the short axis slices obtained in the in vivo myocardial perfusion studies. The slices were stained with Masson's trichrome stain for the perfect identification of fibrosis areas, which are stained in blue.

For fibrosis area quantification in the histologic studies, the tomographic slices were processed similarly to the ones used in the in vivo perfusion studies. In summary, the images corresponding to the four slice levels in the left ventricular chamber were digitalized with the help of a scanner. A circumferential profile following LV wall conformation was delineated by the ImageJ software, and the linear extension of LV circumference was computed for each slice. The fibrosis-stained myocardial tissue linear extension was also identified and quantified in each slice. The myocardial fibrosis extension, expressed as a percentage of the LV surface area, was calculated by dividing the fibrotic tissue total extension in the four slices by the total LV circumferences extension in the four slices and multiplying the final value by 100.

A single investigator, blind to the results obtained in the in vivo images, quantified the fibrosis areas in histologic studies.

Statistical analysis

The results were expressed as mean and mean standard deviation. The variable Gaussian distribution was verified by the Kolmogorov-Smirnov test. The paired t Student test was used for comparing the mean in vivo and histologic myocardial fibrosis extension values. The linear regression test and least square method were used for analyzing the correlation between the individual results obtained with each method. The Bland-Altman graphic method was used for additional concordance analysis between the fibrosis area measurements obtained by the two employed methods.

Results

Spatial resolution of tomographic images

Figure 2B shows the tomographic images of the micro-Jasczak phantom radioactivity filled bars reconstructed from the transversal slices, in a section perpendicular to the long axis. In a visual semi quantitative analysis, it is possible to clearly identify the contours of the group bars with internal diameters of 2 mm, though the image resolution is lost at 1 mm internal diameter, which suggests that the spatial resolution limit is within the 1-2 mm range. More precise spatial resolution determination was possible by analyzing the count profile from a linear source (PSF), which led to a 1.5 mm spatial resolution (full width at half maximum). The pixel size in the imaged object was 0.6 mm.

Visual analysis of the myocardial perfusion images

Figure 3 shows images of the myocardial perfusion SPECT of one of the control animals, used for the initial imaging visualization standardization. High target-organ/background count ratio was observed; the wall limits and LV chamber delineation, as well as RV walls in some of the medium-chamber slices, were clearly visualized. The control animals' images show uniform distribution of the radiotracer among different myocardial follow-ups, with the exception of the apex, which showed smaller uptake intensity,

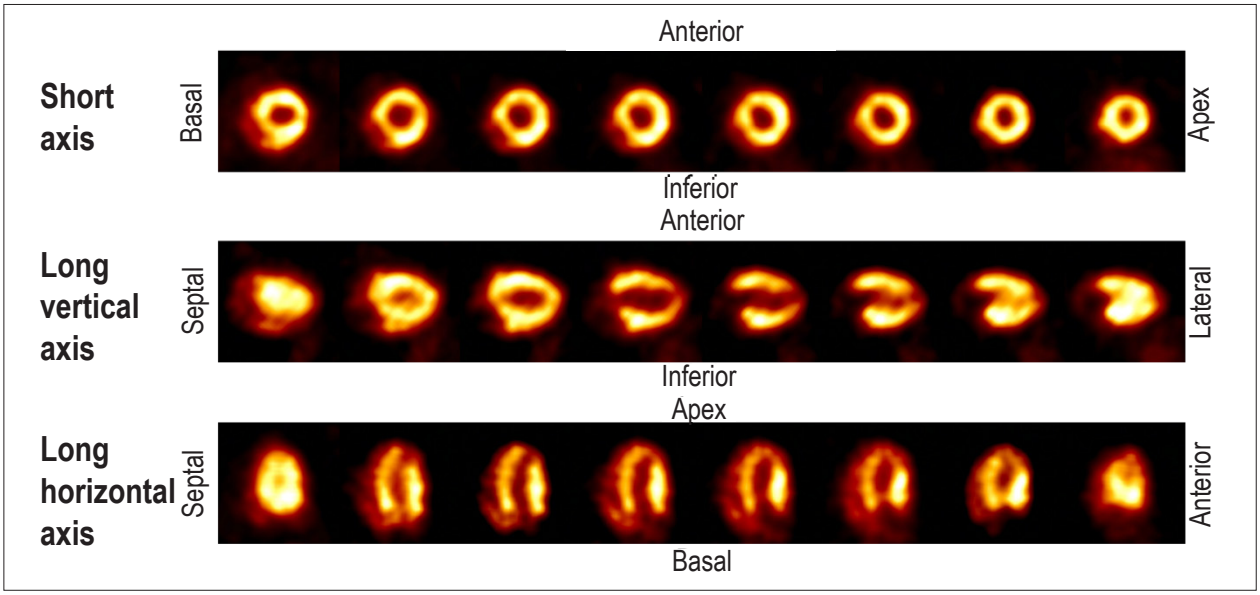

Figure 3 – *Short axis (superior line), horizontal long axis (medium line) and vertical long axis slices of a scintigraphic myocardial perfusion study of one control rat. Image quality comparable to clinical images with good target-organ/background ration, perfect left ventricular wall and chamber visualization, as well as right ventricular wall visualization in some slices*

ascribed to the parietal thinning of the apical region. However, these values were not inferior to 50% in comparison to the maximum myocardial uptake accumulation pixel.

The image quality of the infarcted animals (Figure 4) and the control animals is comparable; besides, the uptake defect was clearly identified in territories compatible with the left coronary artery irrigation area in the rat (anterior and anterolateral walls and apical region) in all animals, with significant infarct areas confirmed by histology.

Quantitative analysis of the myocardial infarction areas

In Figure 5, we can compare SPECT myocardial perfusion tomographic images of the slices with the corresponding histologic images that were used for quantifying, respectively, the perfusional defect and the fibrosis area. Great similarity of the wall morphology, as well as the myocardial perfusional defect extension and topography, can be seen between SPECT images and histologic studies.

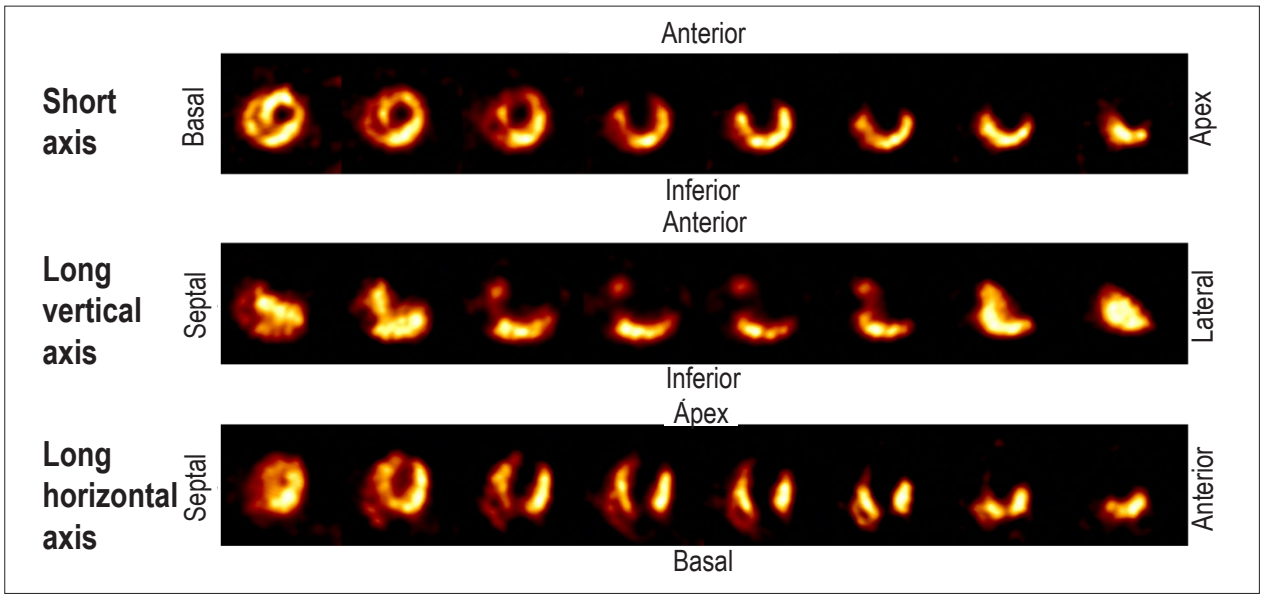

Figure 4 – *Short axis (superior line), horizontal long axis (medium line) and vertical long axis slices of a scintigraphic myocardial perfusion study of a rat with an experimental infarct. Left ventricle chamber dilation and an extensive and severe uptake defect, involving the anterior and anterolateral walls and apical regions can be seen.*

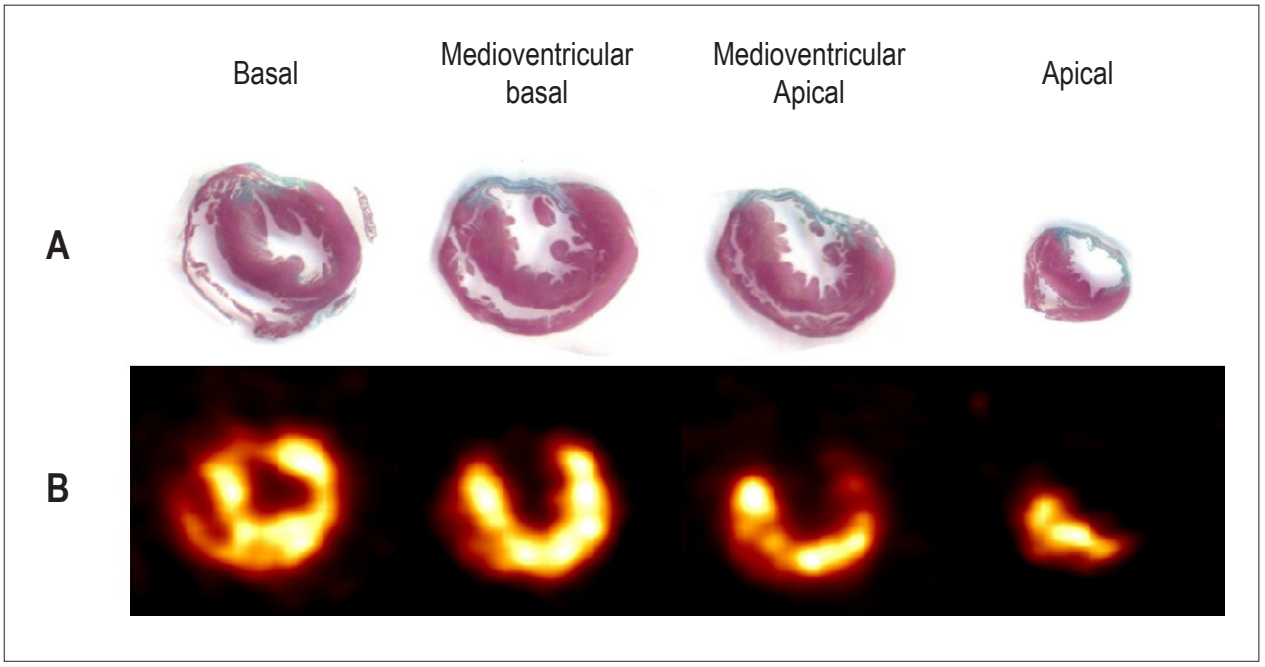

Figure 5 – *An example of the infarct area topographic and quantitative correlation. Histopathologic slices stained by Masson's trichrome (A) and myocardial perfusion SPECT tomographic slices (B) are presented. A severe and extensive perfusional defect at the left ventricle apex and anterior and anterolateral walls with perfect correlation to histology can be seen. The extent of the uptake defect seen on SPECT images (%) is very similar to the fibrosis extent at histopathologic studies (%).*

The myocardial infarction area quantified by histology was 21.7 ± 22.0% of the LV surface. The myocardial infarct area dimensions showed great variation among animals, ranging from 26.5 to 55.0%. Six animals did not show significant fibrosis areas in the histopathologic study.

All the animals with significant myocardial fibrosis in the histopathologic study were correctly identified by the presence of uptake defects in myocardial perfusion defects. The LV surface area in which an uptake defect detected at the myocardial perfusion SPECT (infarct area) was 21.1 ± 21.2% (ranging from 30.0 to 50.0%); the results were similar to the obtained in the histologic study (p=0.45).

Excellent correlation was obtained between individual SPECT myocardial uptake defect values and histologic myocardial fibrosis extension by using linear regression analysis (n = 13. r = 0.99; p < 0.0001). In the dispersion graphic, a slope=1.03, almost superimposed to the identity line between the results, can be seen (Figure 6).

High concordance between the results of both methods is showed by plotting the data according to the graphic method for Bland-Altman measurement concordance analysis (Figure 7). As the graphic shows, the mean difference between measurements was -0.6, a value close to zero (the ideal value). The individual values of the measurement differences are distributed in a narrow range around the mean, within the representative bars of two standard deviations, demonstrating that the variation limit for the difference between measurements was fairly acceptable (±5,4%).

Discussion

In this study, we describe a system for obtaining high resolution SPECT images in small animals based on a pinhole collimator coupled to a rotational support and adapted to a clinical gamma-chamber. To the best of our knowledge, this is the first time an equivalent device is developed in Latin America. This system's performance allowed identifying 1-2 mm structures with 1.5 mm spatial resolution (FWHM) and a 0.6 mm pixel size. These values are similar to the ones reported in other studies describing systems adapted in clinical gamma-camera [13-15] and systems especially built for small animals[16-18].

In addition to their high spatial resolution, the myocardial perfusion SPECT images obtained both from infarct and control animals achieved quality comparable to human images, with adequate visualization of the left ventricle walls and chamber, as well as right ventricle wall visualization in some slices, with a high target-organ/background count ratio.

The wall morphology and infarct area topography, according to myocardial perfusion SPECT images of the animals submitted to experimental infarct, were very similar to the ones obtained in the histopathologic study. Additionally,

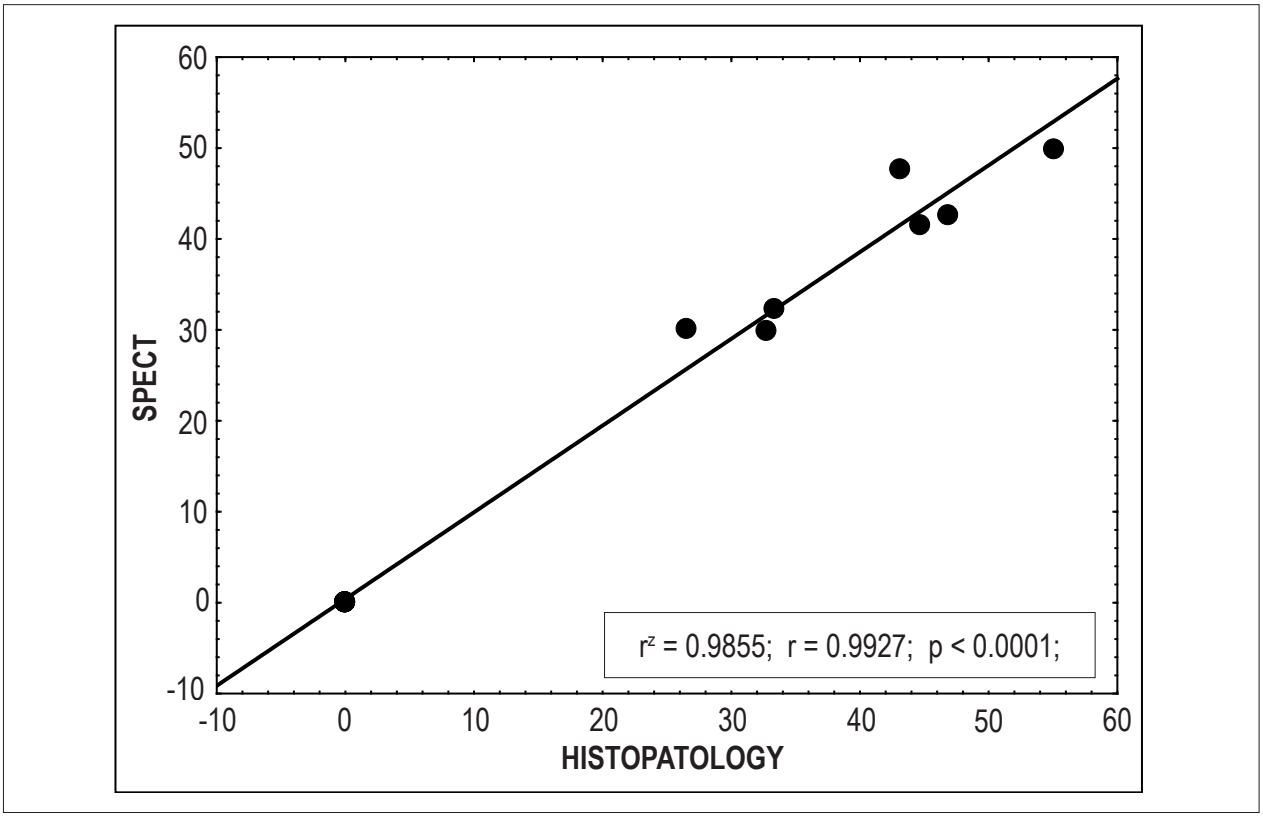

Figure 6 – *Dispersion graphic illustrating the correlation between myocardial infarct areas estimated by the perfusion defects extension (Y axis) and the myocardial fibrosis area according to histopathology (X axis). A high correlation level can be seen r2= 0.98; r=0.99; p< 0.0001.*

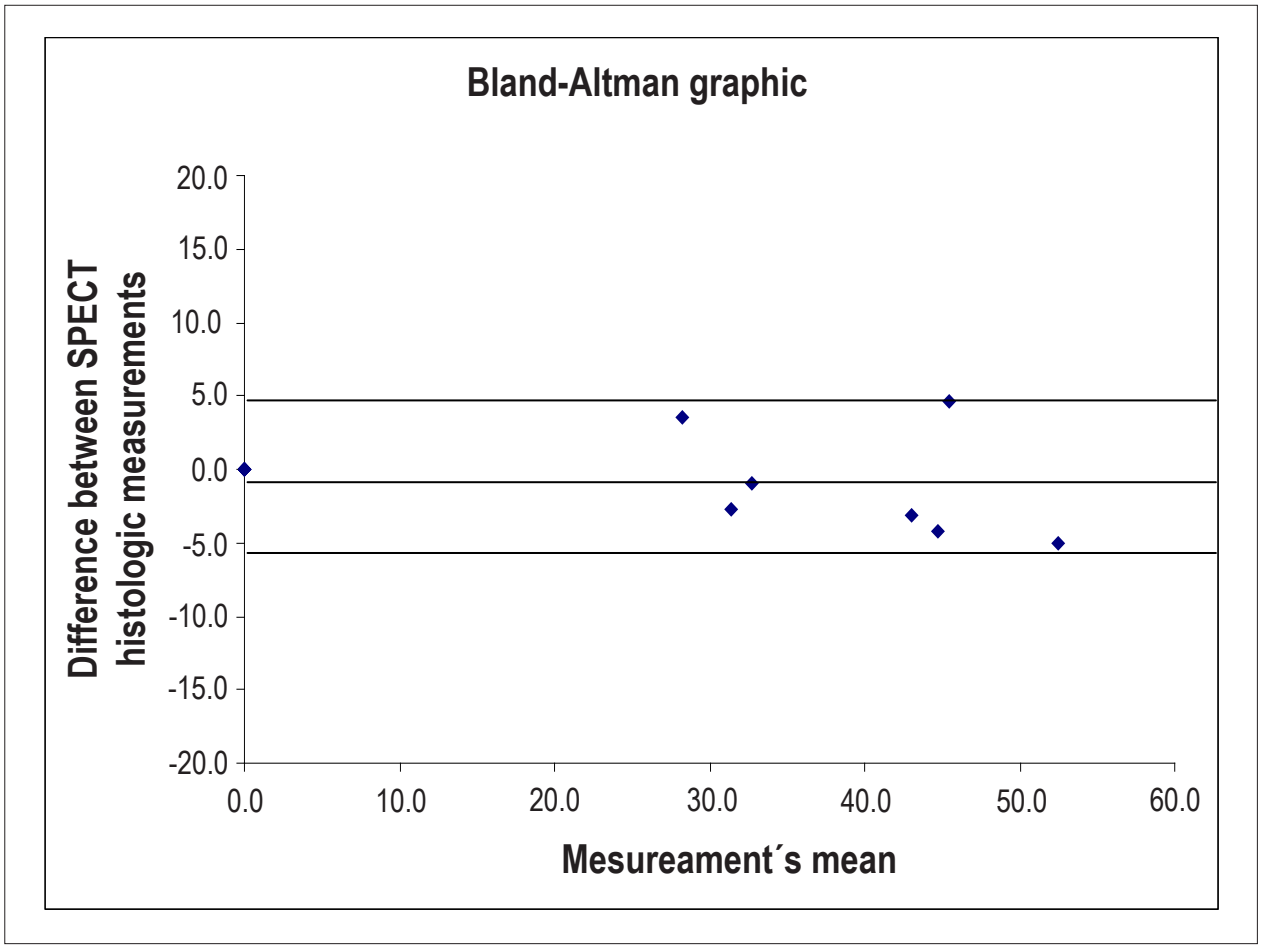

Figure 7 – *Illustration of the Bland-Altman graphic analysis for comparison of myocardial infarct areas measured by SPECT and histology. All data pairs of the difference between values are distributed around the mean (-0.6%) and within 2 standard deviations ((±5.4%) No correlation was found among the values of the difference of measurements and their respective mean values.*

the myocardial perfusion defect extension showed high correlation with the infarct area histologic measurement. Regarding accuracy in the quantification of the infarct area extension, our results are comparable to the ones reported in other studies in with rats and mice were used with other high resolution scintigraphic imaging systems[13,14,18-20]. The findings suggest that, as a whole, the system's performance and accuracy is comparable to the commercially available dedicated systems.

An open architecture imaging system, such as the one described here, is very versatile, since, besides being easily coupled to other gamma-camera, it allows, with small configuration changes, imaging different sized animals ranging from 30 to 800 g. These changes consist in changing the rotational support to others with different widths and adjusting the distance between the animal to be studied and the pinhole, leading to different magnification of the imaged object. This versatility allows also adjusting for the optimization of the imaging parameters of different modalities of cardiac scintigraphic studies in the same animal (e.g., tomographic and planar nuclear ventriculography and perfusion gated-SPECT) and for obtaining functional imaging of different organs (e.g., brain, kidney, thyroid and lungs). Besides, when compared to the commercially available SPECT imaging systems dedicated to small animals, the construction costs of the system described here are incomparably smaller. Approximately $ 5,000 was invested in the materials and the skilled labor employed in its physical assemblage. The reconstruction software development employed freeware platforms and the mathematical formulas and algorithms of the software had been previously published[7].

Other additional technical aspect must be presented in order to explain the advantages of configuring this kind of imaging system, in which the target (the small animal) is rotated in front of the detector. SPECT images are based on the acquisition of a planar images (projections) set in different angles around an object. In a clinical scenario, the projections are usually obtained by parallel collimators, so that the detector head rotates circumferentially around the patient, yielding images with a spatial resolution of approximately 6 mm (width at half the height)[21]. In order

to image small animals' organs, it is technically more advantageous to rotate the animal, and not the detector, for obtaining the projections. This way, most misalignments and oscillations caused by the gamma-camera detector head movement are eliminated, and the construction costs and the system's operation space are minimized.

Differently from what happens when parallel hole collimators are used, there is an implicit magnification factor of the pinhole collimator. This magnification is related to the ratio between the distances of the detector and collimator and the target object and the collimator. The closer the pinhole, the greater the magnification factor of the object being studied. It is also important to highlight that the system's sensitivity (the count accumulation rate) is a function of the collimator hole area. With our equipment, it is possible to used different lead or gold hole diameters (ranging from 0.5 to 2.0 mm), as well as multiple hole collimators, which can optimize the scintigraphic imaging process.

Various points can be selected to highlight the importance of high resolution perfusion imaging in ischemia/reperfusion and ischemic cardiopathy experimental models. Myocardial infarct induction is the heart failure/left ventricular dysfunction model most frequently used in pre-clinical research[22]. The precise quantification of fibrosis extension using imaging methods in vivo may be relevant for characterizing such models, allowing the selection of more homogeneous animals regarding infarct size, as well the longitudinal assessment of the effect of anti-ischemic therapies and myocardial reperfusion strategies, similarly to the described in myocardial perfusion SPECT clinical studies[23].

On the other side, the sequential evaluation of the infarct area dimensions is a critical aspect of the studies on stem cell therapies for myocardial regeneration, much in the same way it has been employed in recent clinical studies[24,25].

It is relevant to mention that echocardiography has been broadly used in pre-clinical research, not only for estimating myocardial infarct dimensions, but also for measuring the subsequent left ventricle remodelation degree[26].

However, it must be highlighted that the utilization of imaging methods that evaluate left ventricular systolic function for measuring indirectly the myocardial infarct extension is subject to various factors that can lead to inaccuracy. The estimation of the myocardial infarct dimensions by the contractile dissinergy area extension can be contaminated by confounding factors, such as the presence of viable, but transiently dysfunctional, myocardium (stunned myocardium) and the change in the vicarious contractile activity degree of the walls distant from the infarct area. These factors can mask the results of therapies aimed at ischemic myocardial salvage or those acting on cardiac remodeling[27].

Thus, the central aspect involved in the comparison of different methods for evaluating infarct size is that myocardial perfusion SPECT can evaluate functionally the extension of viable myocardium and, consequently, the extension of necrotic myocardium. This direct functional/metabolic evaluation does not depend on the wall mobility status, that is, even stunned areas would be judged viable and "tethered" myocardium (fibrosis/necrosis areas exhibiting mobility since they are anchored in circumjacent segments with enhanced contractility) would be correctly judged necrotic. So, reproducing what the international literature has demonstrated in clinical studies, according to our judgment, the scintigraphic functional/metabolic assessment adds important information to the diagnosis of viable myocardium and, by extension, myocardial necrosis, in addition to the information provided by segmental mobility. We believe, thus, that myocardial perfusion SPECT would be an additional tool to echocardiogram (which is still the standard method for measuring the systolic dysfunction and remodeling degree) for more complete evaluation of the ischemic cardiopathy models, as well as measuring the impact of myocardial regeneration cell therapies.

Conclusion

The system developed by us showed high spatial resolution and accuracy in the detection and quantification of myocardial fibrosis areas. It is a low cost tool with great versatility for high resolution SPECT imaging of small animals' organs.

The technological improvements described and validated in the present study may potentially contribute to the popularization of scintigraphic functional assessment in the pre-clinical cardiologic research in the Brazilian scientific setting.

Funding

The preset study was funded by the São Paulo research Foundation (FAPESP), processes 07/50339-3 and 2011/03261-4, by the Teaching and Assistance Foundation (FAEPA) of the Clinical Hospital of the Medical School of Ribeirão Preto (HCFMRP), São Paulo University (USP) and National Council for Scientific and Technological Development (CNPq). JM was granted a scholarship of the Emergent Centers' Young Researcher Support System.

Author contributions

Conception and design of the research: Mejia J, Galvis-Alonso OY, Simões MV; Acquisition of data: Oliveira LFL, Mejia J, Carvalho EEV, Lataro RM, Frassetto SN, Fazan Jr. R, Salgado HC; Analysis and interpretation of the data: Oliveira LFL, Carvalho EEV, Lataro RM, Simões MV; Statistical analysis: Oliveira LFL, Carvalho EEV; Obtaining funding: Mejia J; Writing of the manuscript: Oliveira LFL; Critical revision of the manuscript for intellectual content: Oliveira LFL, Mejia J, Galvis-Alonso OY, Simões MV.

Potential Conflict of Interest

No potential conflict of interest relevant to this article was reported.

Sources of Funding

This study was partially funded by FAPESP, FAEPA-HCFMRP and CNPq.

Study Association

This article is part of the thesis of master submitted by Luciano Fonseca Lemos de Oliveira, from Faculdade de Medicina de Ribeirão Preto – USP.

References

1. Institute of Laboratory Animal Resources (U.S.). Committee on Rodents. Rodents. Washington, DC: National Academy Press; 1996.
2. Tucci PJ. Pathophysiological characteristics of the post-myocardial infarction heart failure model in rats. Arq Bras Cardiol. 2011;96(5):420-4.
3. Zornoff LA, Paiva SA, Minicucci MF, Spadaro J. Experimental myocardium infarction in rats: analysis of the model. Arq Bras Cardiol. 2009;93(4):434-40, 426-32.
4. Dornas WC, Oliveira TT, Augusto LE, Nagem TJ. Experimental atherosclerosis in rabbits. Arq Bras Cardiol. 2010;95(2):272-8.
5. Klocke R, Tian W, Kuhlmann MT, Nikol S. Surgical animal models of heart failure related to coronary heart disease. Cardiovasc Res. 2007;74(1):29-38.
6. Mejia J, Galvis-Alonso OY, Braga J, Correa R, Leite JP, Simões MV. Methodological approaches to planar and volumetric scintigraphic imaging of small volume targets with high spatial resolution and sensitivity. Braz J Med Biol Res. 2009;42(8):692-9.
7. Mejia J, Galvis-Alonso OY, Castro AA, Braga J, Leite JP, Simões MV. A clinical gamma camera-based pinhole collimated system for high resolution small animal SPECT imaging. Braz J Med Biol Res. 2010;43(12):1160-6.
8. Shepp LA, Vardi Y. Maximum likelihood reconstruction for emission tomography. IEEE Trans Med Imaging. 1982;1(2):113-22.
9. Chatziioannou A, Qi J, Moore A, Annala A, Nguyen K, Leahy R, et al. Comparison of 3-D maximum a posteriori and filtered backprojection algorithms for high-resolution animal imaging with microPET. IEEE Trans Med Imaging. 2000;19(5):507-12.
10. Frese T, Rouze NC, Bouman CA, Sauer K, Hutchins GD. Quantitative comparison of FBP, EM, and Bayesian reconstruction algorithms for the IndyPET scanner. IEEE Trans Med Imaging. 2003;22(2):258-76.
11. Loening AM, Gambhir SS. AMIDE: a free software tool for multimodality medical image analysis. Mol Imaging. 2003;2(3):131-7.
12. Pfeffer MA, Pfeffer JM, Fishbein MC, Fletcher PJ, Spadaro J, Kloner RA, et al. Myocardial infarct size and ventricular function in rats. Circ Res. 1979;44(4):503-12.
13. Habraken JB, de Bruin K, Shehata M, Booij J, Bennink R, van Eck Smit BL, et al. Evaluation of high-resolution pinhole SPECT using a small rotating animal. J Nucl Med. 2001;42(12):1863-9.
14. Wu MC, Gao DW, Sievers RE, Lee RJ, Hasegawa BH, Dae MW. Pinhole single-photon emission computed tomography for myocardial perfusion imaging of mice. J Am Coll Cardiol. 2003;42(3):576-82.
15. Moons CP, Peremans K, Vermeire S, Vandermeulen E, Dobbeleir A, Hermans K, et al. The Use of HiSPECT to Investigate Dopaminergic Involvement in the Development of Stereotypic Behaviour. Scand J Lab Anim Sci. 2008;35(4):221-9.
16. Liu ZL, Kastis GA, Stevenson GD, Barrett HH, Furenlid LR, Kupinski MA, et al. Quantitative analysis of acute myocardial infarct in rat hearts with ischemia-reperfusion using a high-resolution stationary SPECT system. J Nucl Med. 2002;43(7):933-9.
17. MacDonald LR, Patt BE, Iwanczyk JS, Tsui BM, Wang YC, Frey EC, et al. Pinhole SPECT of mice using the LumaGEM gamma camera. IEEE Trans Nucl Sci. 2001;48(3):830-6.
18. Wollenweber T, Zach C, Rischpler C, Fischer R, Nowak S, Nekolla SG, et al. Myocardial perfusion imaging is feasible for infarct size quantification in mice using a clinical single-photon emission computed tomography system equipped with pinhole collimators. Mol Imaging Biol. 2010;12(4):427-34.
19. Hirai T, Nohara R, Hosokawa R, Tanaka M, Inada H, Fujibayashi Y, et al. Evaluation of myocardial infarct size in rat heart by pinhole SPECT. J Nucl Cardiol. 2000;7(2):107-11.
20. Acton PD, Thomas D, Zhou R. Quantitative imaging of myocardial infarct in rats with high resolution pinhole SPECT. Int J Cardiovasc Imaging. 2006;22(3-4):429-34.
21. Cherry SR, Sorenson JA, Phelps ME. Physics in nuclear medicine. 3rd ed. Philadelphia, PA: Saunders; 2003.
22. Monnet E, Chachques JC. Animal models of heart failure: what is new? Ann Thorac Surg. 2005;79(4):1445-53.
23. Gibbons RJ. Tc-99m SPECT sestamibi for the measurement of infarct size. J Cardiovasc Pharmacol Ther. 2011;16(3-4):321-31.
24. Strauer BE, Brehm M, Zeus T, Kostering M, Hernandez A, Sorg RV, et al. Repair of infarcted myocardium by autologous intracoronary mononuclear bone marrow cell transplantation in humans. Circulation. 2002;106(15):1913-8.
25. Perin EC, Willerson JT, Pepine CJ, Henry TD, Ellis SG, Zhao DX, et al. Effect of transendocardial delivery of autologous bone marrow mononuclear cells on functional capacity, left ventricular function, and perfusion in chronic heart failure: the FOCUS-CCTRN trial. JAMA. 2012;307(16):1717-26.
26. Minicucci MF, Azevedo PS, Matsubara BB, Matsubara LS, Paiva SA, Zornoff LA. [Association between sphericity, ventricular function and size of the infarction in rats]. Arq Bras Cardiol. 2010;94(5):645-50.
27. Botker HE, Kaltoft AK, Pedersen SF, Kim WY. Measuring myocardial salvage. Cardiovasc Res. 2012;94(2):266-75.